Available online at www.sciencedirect.com
ScienceDirect
J. Mater. Sci. Technol., 2012, **28**(3), 255–260.
JMST
www.JMST.org

Microhardness, Microstructure and Electrochemical Efficiency of an Al (Zn/xMg) Alloy after Thermal Treatment

Socorro Valdez[1)†], *M. Suarez*[2)], *O.A. Fregoso*[2)] *and J.A. Juárez-Islas*[2)]
1) Instituto de Ciencias Físicas-UNAM, Av. Universidad S/N Col. Chamilpa, 062210, Cuernavaca, Morelos, México
2) Instituto de Investigaciones en Materiales-UNAM, Circuito escolar S/N, Cd. Universitaria, 04515, México, D.F., México
[Manuscript received August 10, 2011, in revised form September 20, 2011]

The influence of Mg on the microhardness, microstructure and electrochemical efficiency of Al(Zn/xMg) alloys have been investigated. Al(Zn/xMg) alloys were prepared by metal mould casting method to diminish the process cost and to generate an alloy with homogenous microstructure and less casting porosity. Vickers hardness, X-ray diffraction, scanning electron microscopy and transmission electron microscopy were performed to determine the Mg influence on the AlZn alloy. Electrochemical efficiency was used to relate the influence of Mg with the thermal treatment on the corrosion behavior of the Al(Zn/xMg) alloy. The results reveals the presence of $Al_{32}(MgZn)_{49}$ phase for two events; the first is when the Mg content is above 5.49% in as-cast condition, and the second after the thermal treatment is carried out at 450 °C for 5 h. The results also show that the microhardness and electrochemical efficiency have been influenced by the presence of $Al_{32}(MgZn)_{49}$ phase. The addition of Mg modifies the microstructure, increases the content of $Al_{32}(MgZn)_{49}$ phase and improves the electrochemical efficiency.

KEY WORDS: Al(Zn/xMg) alloy; Microhardness; Electrochemical efficiency; Microstructures

1. Introduction

The Al-base alloys, specially the AlZn alloys are widely used in automobile engine, drive trains, agriculture equipment, transportation, packaging, aerospace, construction and other high-tec industries[1]. These alloys combine their mechanical properties like ductility and conformability with their low density, excellent castability, resistance to corrosion, high hardness and high specific strength[2]. This kind of alloys are considered as an effective substitute of ferrous and nonferrous materials[1]. It is well known that the ternary Al–Zn–Mg alloys are widely used in aerospace applications due to the unique combination of lightweight and high mechanical properties[3]. The last property has been improved by the strong age-hardening after their heat treating[4]. This alloy has also been considered as galvanic anode due to their anodic dissolution process showing a more negative (or active) corrosion potential[5]. The anodic activation of Al(Zn/xMg) alloy has been obtained with elements such as In, Sn, Hg and Bi. These activators are in solid solution or as segregated phase[6] and also as intermetallic phases formed precipitation after heat treatment[7]. The precipitation process in Al-base alloys indicates a several transformation sequences during ageing[8]. Heat treatment relies on the fine precipitation from the supersaturated solid solution (SSS), and precipitation is associated with nucleation and growth process. In our case, the precipitates are the $Al_{32}(MgZn)_{49}$ and $MgZn_2$ phases from the α-aluminum matrix. These precipitates strained the crystallographic planes of the Al matrix[9]. However, the microhardness and electrochemical efficiency as sacrificial anode are critically dependent on composition and microstructure. Microstructure is developed during casting, thermomechanical processing

† Corresponding author. Prof., Ph.D.; Tel.: +52 777 3291785; Fax: +52 777 3291745; E-mail address: svaldez@fis.unam.mx (S. Valdez).

and heat treatment[10]. It is well known that the microstructure is essential for the properties of alloys. However the relationship between microstructure plus electrochemical efficiency and microhardness of Al(Zn/xMg) alloys has been seldom studied[10,11]. With all this in mind, in this work the ability of Mg as an anodic activator has been considered because Mg is the most active metal in the galvanic series and Mg alloying is always the active anode when it contacts other metals[12]. The aim of the present study is to understand better the influence of Mg on the AlZn microstructure, microhardness and electrochemical efficiency. Microstructure was studied using scanning electron microscopy (SEM) with an energy dispersive X-ray (EDX) analysis, X-ray diffraction (XRD) and transmission elctron microscopy (TEM). The electrochemical behavior was studied by open-circuit potential measurements. The thermal treatment and high Mg content are the principal factors for microstructure changes and also for the electrochemical efficiency and microhardness results. The electrochemical test reveals the susceptibility of AlZnMg alloy with the artificial ageing and quantity of $Al_{32}(MgZn)_{49}$ phase. The distribution of $Al_{32}(MgZn)_{49}$ produces the anodic process activation, which is related with the galvanic efficiency and the microhardness in the Al(Zn/xMg) alloy.

2. Experimental

2.1 Synthesis of Al(Zn/xMg) *alloys and thermal treatment*

Considering that composition and casting conditions will influence the selection and volume fraction of precipitates, certain variables have been taken into account. The AlZn matrix alloy was prepared by stoichiometrically mixing pieces of commercially available elemental Al, Zn and Mg (ingots 99.8% purity). The Al (660 °C), Zn (420 °C) and Mg (650 °C) ingot pieces were melted in a high alumina crucible in a vacuum induction furnace at 700 °C. A constant flux of argon to avoid the contact with the environment and the elements oxidation has been utilized. However, to compensate some oxidation losses during the pour, 3 wt% Al and 7 wt% Zn were taken in excess. Eight different compositions of Mg were added to the AlZn melt alloy. The liquid bath was stirred for 10 min for a uniform distribution of Zn and Mg. The AlZnMg melt was poured into a steel mould to form ingot of 20 mm×50 mm×70 mm. Each ingot was machined to eliminate the structure formed by direct contact with the mould wall. Table 1 shows the nominal chemical composition of Al(Zn/xMg) alloys, obtained by optical emission spectroscopy, using a Spectrolab spectrometer Model X8-Windows Lax with 15 analytical channels, which operates under Microsoft Windows environment. These results are the average of five analyses in different regions of the specimens.

Table 1 Composition of Al(Zn/xMg) alloy under study (wt%)

Alloy	Mg	Zn	Mn	Trace elements	Al
Al-1	3.96	5.36	0.3189	0.1150	Bal.
Al-2	4.89	5.35	0.3125	0.1390	Bal.
Al-3	5.49	5.32	0.3053	0.1287	Bal.
Al-4	6.55	5.32	0.2320	0.1564	Bal.
Al-5	7.33	5.30	0.2931	0.1269	Bal.
Al-6	8.65	5.29	0.2877	0.1343	Bal.
Al-7	9.58	5.29	0.2851	0.1022	Bal.
Al-8	11.53	5.31	0.2178	0.1228	Bal.

To investigate the effect of Mg on the heat treatment and microstructure, samples of 100 g were cut from the cast ingot and were heat treated (homogenization treatment) at 450 °C for 5 h. The temperature and time were determined on the basis of literature data[3] and calorimetric investigations. With the solution heat treated, all solute atoms from soluble phases enrich the solid solution. After that quenching in water at room temperature was carried out to develop supersaturation. The homogenized samples were then artificially aged at 400 °C for 1 h, to start the precipitation process. This is sensitive to the trace or microalloying elements, which can change the process and/or kinetics of precipitation in many age hardenable alloys[13]. Frequently the aging heat treatment involves the formation of finely dispersed precipitates from the supersaturated solid solutions to increase the hardening/strengthening alloy system.

2.2 Metallographic analysis

As-cast and aged samples were sectioned longitudinally at mid-width using a band saw. One side was prepared for microstructural characterization by the standard technique of grinding with SiC up to # 1000 metallographic paper, and mechanical polishing with 0.5 and 0.05 μm alumina powder, followed by etching in Keller′s reagent[14], which contained 5 ml of HNO_3, 3 ml of HCl, 2 ml of HF, and 190 ml of H_2O; the etching was done at room temperature for 15 s. For TEM, foils were taken from the middle-point of each sample at the centre of the cross-sections. After that, the top surface of the samples was mechanically grinded and polished to 70-μm thick and then foils with 3 mm in diameter were selected. The thin foils samples were perforated by jet electropolishing at 12 V using an electrolyte solution[15] of 33 vol.% HNO_3 in methanol, cooled at −17 °C by liquid nitrogen.

2.3 Characterization

Structural investigations were carried out on a Siemens D5000 X-ray diffractometer with a power of 40 kV accelerating voltage and 30 mA current, using Cu tube of $K\alpha$ line radiation: λ=0.15406 nm and a diffracting beam graphic monochrometer. The

XRD patterns were recorded in the 2θ range of 30–90 deg. (step size 0.02 deg., time per step 0.6 s) and the evaluation of the diffractograms was made by DIFRACT/AC software. The Al(Zn/xMg) microstructures were studied using a Stereoscan 440 scanning electron microscope using backscattered electron imaging operated at 20 kV and, a Jeol 2100 transmission electron microscope. SEM and TEM are equipped with an *in situ* energy dispersive X-ray spectrometer (EDS) OXFORD Isis 300.

The Vickers hardness was measured with a microhardness tester INSTRON model 210013 on the cross-sections of the samples using a load of 2 N for l0 s and at least l0 impressions were recorded of each sample. Obtained values were averaged excluding the maximum and the minimum values and the experimental error was estimated.

2.4 Performance evaluation

The galvanic performances of the Al(Zn/xMg) alloys were evaluated by a short-term electrochemical test[15]. The working electrodes, *i.e.* anodes in an oxidation reaction (10 $mm^2 \times 50$ mm length), were prepared from Al(Zn/xMg) ingots of as-cast and aged condition. All the specimens were polished with 1200 emery paper, then degreased in acetone and washed thoroughly in double distilled water. The working electrode used for each test was mounted in a specially designed electrochemical cell, which posseses three-electroded system connected electrochemically to a galvanostat DC current source. A saturated calomel electrode (SCE, E=+0.242 V saturated) was used as the reference electrode. It is used as half cell, and controls the working electrode potential and references the measurement. An auxiliary electrode, from electrochemically inert platinum wire, was used as counter electrode; it functions as cathode (in a half cell) and passes all the current needed to balance the reaction at the working electrode. A sheet of carbon steel served as the cathode. The electrolytic test solution was synthetic sea water, which was prepared with analytical grade reagent sodium chloride and distilled water with an initial pH of 8.3 according to ASTM D1141[16].

The test anode and cathode were galvanically coupled together at different current density levels (0.4, 1.5, 4.0 mA/cm^2) and immersed in the electrolytic solution for 3 d. The anodic current density was applied during a 24-h period. The samples were taken out, and cleaned by ASTM G 31 standard practice. The anodes were then rinsed with distilled water, dried by blowing hot air and weighed to obtained weight loss. The weight of the anode before and after the immersion was measured. From the actual weight loss measured, the capacity and theoretical current or total charge to be produced by the alloy could be calculated. The anode efficiency (η) was calculated by actual ampere hours delivered by Al(Zn/xMg) alloys dividing theorical amperes hours calculated from weight loss of Al(Zn/xMg) alloys.

3. Results and Discussion

3.1 Microstructure investigation

Fig. 1 shows XRD patterns of the Al(Zn/xMg) alloys, in as-cast and ageing thermal treatment condition. Fig. 1(a)–(d) show that the alloys in as-cast and aged condition are composed of α-Al solid solution and $Mg_{32}(AlZn)_{49}$ precipitates, so-called τ-phase particles in this work. The α phase, is a simple face-centered cubic (fcc) α-Al solid solution with an estimated lattice parameter a=0.4049 nm. α-Al is the principal phase for AlZnMg with poor Mg content. When the Mg addition is up to 5.49%, a $Mg_{32}(AlZn)_{49}$ second phase during solidification is favored

The primary precipitate is a body-centered cubic (bcc) $Mg_{32}(Al,Zn)_{49}$ phase also called τ-$Al_2Mg_3Zn_3$ with lattice parameter a=0.1416±0.03 nm. This body cubic phase has a Pearson symbol cI 162 and space group *Im*-3 (No. 204) based on a periodic arrangement of icosahedral Berman clusters[17]. These results are according to the phase diagram[18] when the Mg content is upper to 4.89%. However the intermediate Mg-rich phases Mg_2Al_3 or Mg_5Al_8 with cubic cell a=2.8239 nm, space group Fd-3m were not detected at less atomic concentration. In this case, an incorporation of Mg atoms with crystal structure is hexagonal close-packed (hcp) into the AlZn alloy matrix.

One phase precipitation is suggested by the progressive shifting of (530) and (100) XRD peaks of $Al_{32}(MgZn)_{49}$ phase, from 2θ angles of 36.71–35.3 deg. and 8.80–6.58 deg., formed up to 7.33% Mg content (Fig. 1(a)); this is 1.38 times more than the atomic percentage of zinc, which is nearly constant for all the alloys.

The X-ray diffractograms (left side) in as-cast and aged condition show that $Al_{32}(MgZn)_{49}$ phase precipitates are formed at high Mg addition. However there are few reflections of the $Al_{32}(MgZn)_{49}$ precipitates for the alloy with low Mg content shown in Fig. 1 (right side). These observations demonstrate that the formation of $Al_{32}(MgZn)_{49}$ particles was promoted through the high Mg addition with aged condition. It is apparent also from inspection of Fig. 1 (right side) that the relative intensity for the (111) reflection of the α-Al (which is a rich aluminum solid solution of crystalline structure fcc) is much higher than that of the other peaks. Thereby indicating a preferential crystallographic orientation is developed during the casting operation, even though the XRD intensities are also influenced by the phase content, the crystallite size, lattice strain and degree of crystallinity[19]. During the heat treatment an atomic reordering of the aluminum matrix exists towards a preferential direction of the planes (220) and (311) as it can be observed in Fig. 1(c). The variations in intensity and small

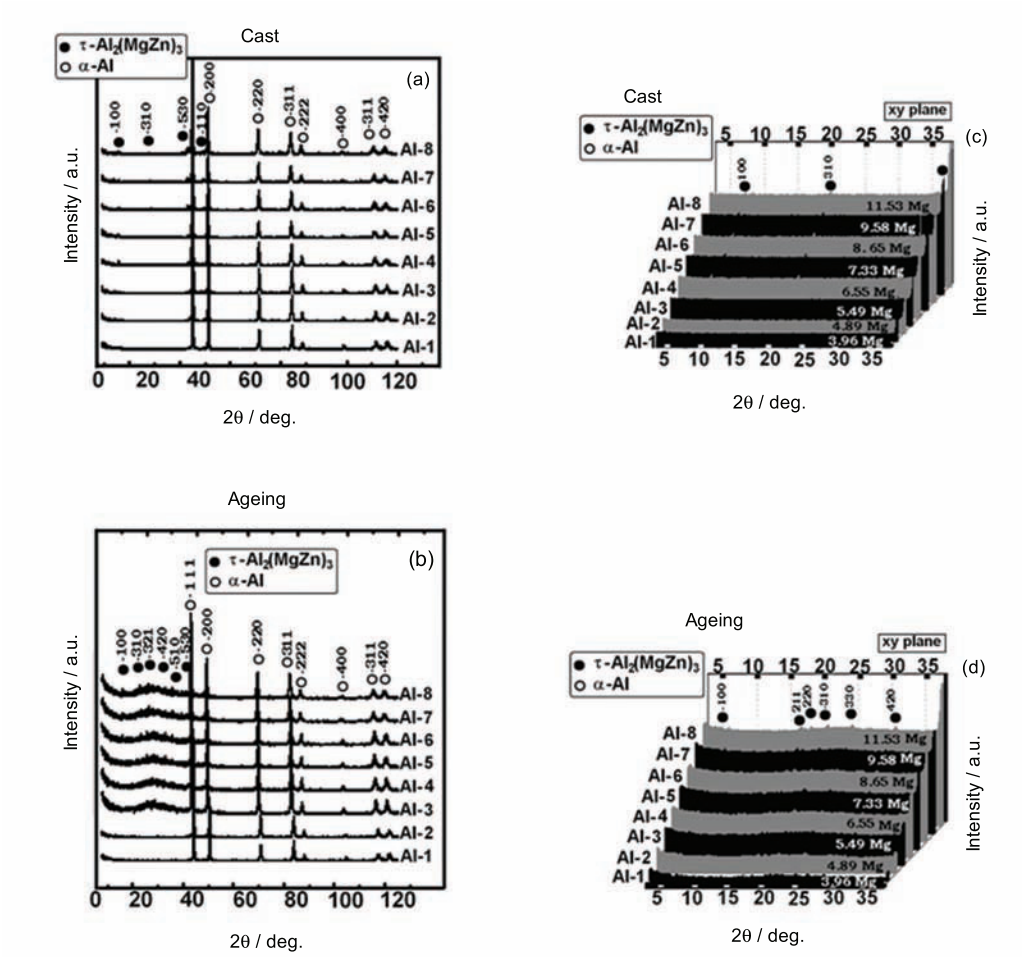

Fig. 1 X-ray diffractograms of the Al(Zn/xMg) alloy in as-cast (a) and (b), and ageing (c) and (d) condition showing the presence of the main lines of diffraction τ-$Al_{32}(MgZn)_{49}$ and α-Al peaks with eight different Mg contents

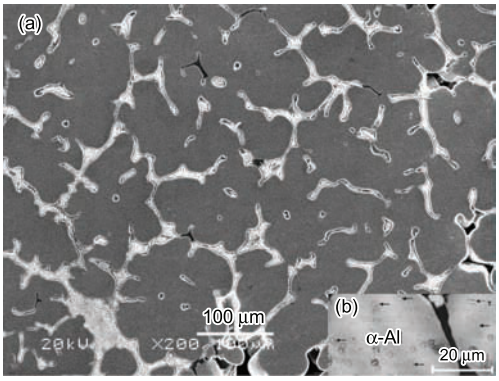

Fig. 2 (a) Microstructure of Al(Zn/xMg) alloys formed by α-Al equiaxed dendritic structure as-cast condition, (b) $Al_{32}(MgZn)_{49}$ precipitation in the matrix aged condition, τ-$Al_{32}(MgZn)_{49}$

displacements of the diffraction angle have their origins from the variations in composition of the alloy probably due to the formation of a supersatured solid solution enriched by solute atoms like Mg and Zn.

The results show the α-Al and $Al_{32}(MgZn)_{49}$ phases formed as products of solidification in the composition range of 7.33 to 11.53 at.% Mg. All the alloys contain α-Al with a dendritic structure developed by the combination of thermal and constitutional undercooling. The representative as-cast microstructure (Fig. 2(a)) reveals the presence of equiaxed morphology structure. In four of the AlZnM alloys from 7.33 to 11.53 at.% Mg, the primary solidification is followed by eutectic solidification of $\alpha+\tau$-$Al_{32}(MgZn)_{49}$ phase. It has been reported[2] that the lamellar eutectic structure is derived from the decomposition of the α' phase by the following cellular reaction at 762 K: $\alpha' \rightarrow \alpha\text{-Al} + Al_{32}(MgZn)_{49}$ or τ-$Al_2Mg_3Zn_3$. Homogeneously dispersed stable $Al_{32}(MgZn)_{49}$ phase as rods precipitates in aged samples were observed (Fig. 2(b)). The heat treatment and high Mg addition caused an increase in the volume fraction of $Al_{32}(MgZn)_{49}$ precipitates.

As-cast structure is modified with heat treatment. It can be observed from the Fig. 3(a) that dendritic

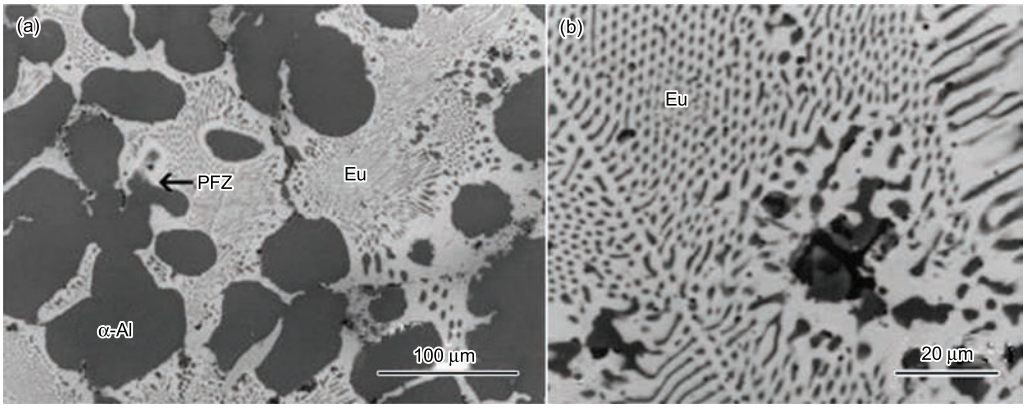

Fig. 3 (a) Quasibinary eutectic of α-Al plus $Al_{32}(MgZn)_{49}$ between the grain boundaries in aged alloys, (b) detail of τ- $Al_{32}(MgZn)_{49}$ phase

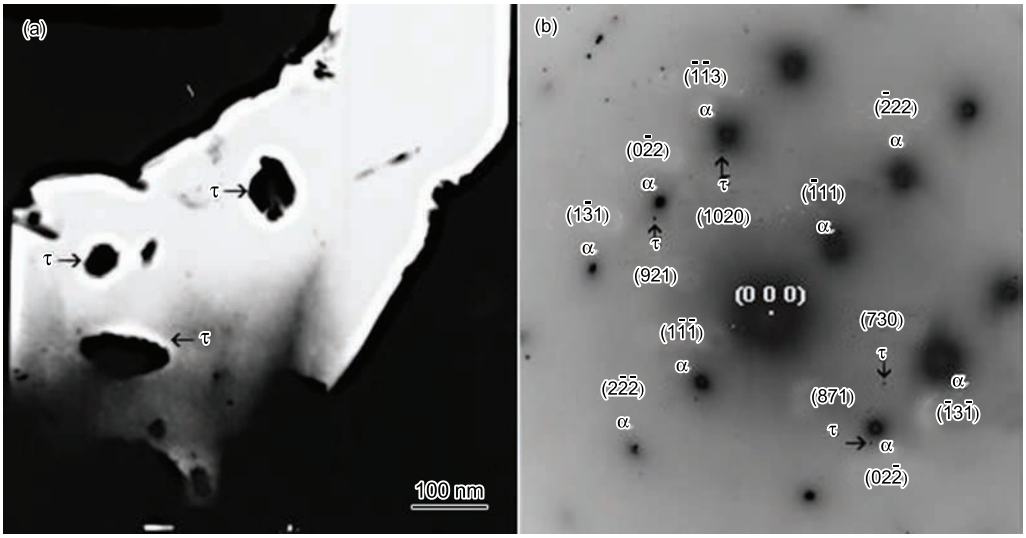

Fig. 4 (a) Precipitates and (b) relative electron diffraction pattern. It can be indexed according to a body cubic center crystalline structure (a=1.416 nm)

structure is broken down and shows a quasibinary eutectic mixture of Al and $Al_{32}(MgZn)_{49}$ along the grain boundaries of primary α-Al grains in aged alloys. In the eutectic region, the light contrast corresponds to $Al_{32}(MgZn)_{49}$, while dark contrast corresponds to the α-Al phase (Fig. 3(b)). The literature on AlZnMg alloys[12,13], point out that the equilibrium situation involves the existence of two principal phases: an aluminum based α-solid solution and the other phase, the τ-$Al_{32}(MgZn)_{49}$, which is considered as a non-stochoimetrically intermetallic phase having a variable composition around the $Al_2Mg_3Zn_3$ formula.

The TEM micrograph shown in Fig. 4(a) represents the microstructures of the $Al_{32}(MgZn)_{49}$ phase in aged alloy preferentially. The indexing of the diffraction pattern (Fig. 4(b)) shows that the lattice parameters of the precipitates are congruent to $Al_{32}(MgZn)_{49}$ phase[14,15].

3.2 Microhardness and electrochemical results

In the previous work[20] the Mg content has been related with the hardness on an Al-alloy, and this relationship was considered to be related with the semicoherent and coherent Mg precipitates. The precipitates can interact with the α-Al matrix and effectively impede dislocation motion. In our case, the $Al_{32}(MgZn)_{49}$ precipitate and the matrix alloy form a connection between the hardness and crystallographic structure. The relationship is influenced by the bcc and fcc crystal structure. Another effect could be the atomic size of alloying elements, because Zn and Mg are smaller and larger, respectively than Al[4]. In addition, the presence of $Al_{32}(MgZn)_{49}$ precipitates is also associated with the galvanic efficiency due to the difference in the electrical potential between these precipitates and the matrix. The precipitates permit a galvanic activity continued avoiding the polarization of the alloys, which allow to act as sacrificial anodes.

Microhardened and anode efficiency curves in as-cast and aged condition are shown in Fig. 5. The α-Al aged structure is 8% harder than the surrounding Al-matrix in as-cast alloys. Indeed, the average Vick-

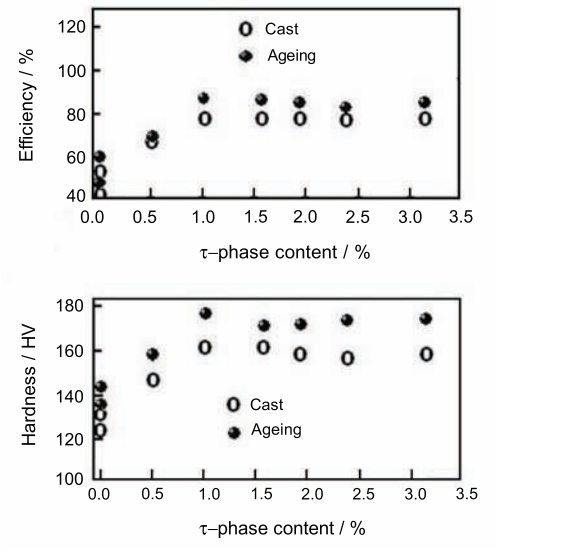

Fig. 5 Hardness and anode efficiency plotted against τ-$Al_{32}(MgZn)_{49}$ phase curves for the alloys Al(Zn/xMg) in as-cast and aged condition

ers hardness measured inside the Al-matrix in cast structure is 83.65 HV, whereas the Al-matrix aged is 91.81 HV. These values emphasize the influence of the $Al_{32}(MgZn)_{49}$ particles inside the matrix. It can be seen from Fig. 5 that the alloy with 1.0% of τ-phase content and with 5.49% Mg addition had a great hardening and galvanic efficiency. These properties are developed at 1.0 vol.% $Al_{32}(MgZn)_{49}$ phase particles. The peak efficiency is achieved after 4.89% Mg addition and 0.5% of τ-phase content. The efficiency curve for as-cast condition show the similar behavior: the high peak is reached when $Al_{32}(MgZn)_{49}$-phase is equal to 1.0 vol.%. It is clear that ageing treatment enhances the peak hardness and efficiency when Mg addition does not exceed 5.49%, which corresponds to 1.0% of τ-phase content. It means that $Al_{32}(MgZn)_{49}$ phase increases due to the formation of quasibinary eutectic structure (α-Al + $Al_{32}(MgZn)_{49}$). While for the α-matrix their hardness decreases and also their $Al_{32}(MgZn)_{49}$ precipitate distribution. These results emphasize that precipitates influenced the electrochemical efficiency. The efficiency is greater when the initial attack is present for the intermetallic compounds distributed in the matrix, however the intergranular eutectic phase begins to dissolve and the intergranular corrosion is stronger than the $Al_{32}(MgZn)_{49}$ phase.

4. Conclusions

(1) The precipitation of $Al_{32}(MgZn)_{49}$ particles depends on the Mg addition, ageing condition and the quantity of the eutectic phase formation.

(2) The addition of Mg in just 5.49 at.% to the ageing AlZn alloy clearly increases the peak efficiency and generates the 1.0 vol.% $Al_{32}(MgZn)_{49}$ precipitates.

(3) For Mg content above than 5.49% with ageing, the eutectic phase increases more than $Al_{32}(MgZn)_{49}$ precipitates, and the electrochemical efficiency of the alloy decreases while for the allays with low Mg content the phase $Al_{32}(MgZn)_{49}$ and the efficiency have been decreased.

(4) A galvanic efficiency as high as 81% has been achieved with Mg and aged on Al(Zn/xMg) alloy, and the activation process depends on the amount of $Al_{32}(MgZn)_{49}$ particles deposited at the Al-matrix surface.

Acknowledgements

The authors thank Consejo Nacional de Ciencia y Tecnología (CONACyT) under Grant No. 89981 and UNAM-PAPIIT through research under Grant No. INI05708 for the financial support.

REFERENCES

[1] T. Pervez, S.Z. Qamar, A.C. Seibi and F.K. Al-Jahwari: *Mater. Design*, 2008, **29**, 811.
[2] H. Khalid Rafi, G.D. Janaki Ram, G. Phanikumar and K. Prasad Rao: *Mater. Des.*, 2010, **31**, 2375.
[3] L.F. Mondolfo: *Aluminium alloys: Structure and Properties*, Butterworths, London, 1971, 953.
[4] G. Mrówka-Nowotnik and J. Sieniawski: *J. Mater. Process. Technol.*, 2005, **162–163**, 367.
[5] S. Valdez, B. Mena, J. Genesca and J.A. Juárez-Islas: *J. Mater. Eng. Perform.*, 2001, **10**, 596.
[6] S.M.A. Shibli: *Corros. Sci.*, 2004, **46**, 819.
[7] F. Eckermanna, T. Suter, P.J. Uggowitzer, A. Afseth and P. Schmutz: *Electrochem. Acta*, 2008, **54**, 844.
[8] Z.H. Li, B.Q. Xiong, Y.A. Zhang, B.H. Zhu, F. Wang and H.W. Liu: *Mater. Charact.*, 2008, **59**, 278.
[9] I.J. Polmear: *Light Alloys, Metallurgy of the Light Metals*, 2nd edn, Arnold, London, 1989, 21.
[10] H. Ezuber, A. El-Houd and F. El-Shawesh: *Mater. Des.*, 2008, **29**, 801.
[11] M.A. Talavera, S. Valdez, J.A. Juarez-Islas, B. Mena and J. Genesca: *J. Appl. Electrochem.*, 2002, **32**(8), 897.
[12] G.L. Song, B. Johannesson, S. Hapugoda and D. StJohn: *Corros. Sci.*, 2004, **46**, 955.
[13] S.P. Ringer and K. Hono: *Mater. Charact.* 2000, **44**(1–2), 101.
[14] K. Mills, J.R. Davis and J.D. Destefani: *ASM Handbook, Vol. 9: Metallography and Microstructure*, ASM International, USA, 1998, 354.
[15] DNV Recommended Practice RP B401 (1993): *Cathodic Protection Design*, Det Norske Veritas Industry As, Hovik, 1993.
[16] ASTM D1141–98: *Standard Practice for the Preparation of Substitute Ocean Water, Annual Book of ASTM Standards*, American Society for Testing and Materials, Philadelphia, Pennsylvania, USA, 2004.
[17] G. Bergmaiv, J.L.T. Waugh and L. Pauling: *Acta Cryst.*, 1957, **10**, 254.
[18] V. Raghavan: *J. Phase Equilib.*, 2007, **28**(2), 203.
[19] B.D. Cullity: *Elements of X-ray Diffraction*, 2nd edn, Addison-Wesley Publishing Company, Inc., MA, USA, 1978.
[20] L.A. Dobrzanski, T. Tanski, J. Trzaska and L. Cizek: *J. Achievements. Mater. Manufact. Eng.* 2008, **26**, 187.